Chapter 4

Design and Implementation of Micromechatronic Systems: SMA Drive Polymer Microgripper

Ren-Jung Chang and Yu-Heng Lai

Additional information is available at the end of the chapter

http://dx.doi.org/10.5772/67266

Abstract

A micromechatronic gripper was designed, fabricated, and tested with the proposed control system. By following realization axioms, the microgripper system including a polyurethane (PU) gripper mechanism and shape memory alloy (SMA) actuator was designed and developed. The micromechatronic gripper system was realized with cross-sectional area of $(\pi/4) \times 500^2$ μm^2 for clean room operation. A synergetic operation of SMA actuator for driving microgripper mechanism was investigated in visual-based control. By incorporating with inverse Preisach compensator, an explicit self-tuning controller through Ziegler-Nichols criterion was selected for controlling the self-biased SMA actuator. The application of the gripper system for gripping and transporting a glass particle of 30 μm was tested.

Keywords: design, control, micromechatronic systems, polymer, gripper

1. Introduction

The area of mechatronics is continually evolving, from Yasakawa's definition in the 1970s, through intelligent mechatronics and optomechatronics in the 1980s, to teleoperation and micromechatronics in the 1990s [1]. In the beginning of the 1970s, mechatronics was viewed as the combination of "mecha" from mechanism and the "tronics" from electronics [2]. Along with the evolution of mechatronics, people in mechatronic engineering used a variety of definitions [1–3]. In 1991, the International Federation for the Theory of Machines and Mechanism (IFToMM) gave the definition of mechatronics as: Mechatronics is the synergetic

combination of precision mechanical engineering, electrical control, and systems thinking in the design of products and processes. This definition had been adopted within the European Economic Community (EEC), which was later incorporated and renamed as the European Community (EC). In the perspective of industrial systems, the constituent components of mechatronic system include mechanism, actuator, sensor, and controller [2, 3]. Thus, by extending the definition of mechatronics and applying it to downscaling mechatronic systems, one may characterize a micromechatronic system as a system consisting of microscale mechanism, actuator, sensor, and controller which are designed and operated synergistically to achieve microoperation [2–4].

Miniaturization of mechatronic system has become a challenging area of technology in robotic and biomedical industries. In a specific area of micromechatronics, a microgripper system has been developed to provide a manipulation tool for the macroworld operation of microworld object. Since the first silicon microgripper was developed and proposed by Kim et al. in 1990 [5], several prototype miniature grippers have been designed and fabricated. The research trend on microgrippers has evolved toward a micromechatronic system by including force sensing and servo control [6–11]. In the industries of information, material, and biomedical engineering, microgrippers that are capable of handling small objects have many important applications [6, 7, 12–15]. In exploiting the compliant design and materials used for gripper mechanism, the researches of microelectromechanical systems (MEMS) [16] and compliant machine [17, 18] have stimulated the interests on implementing compliant microgripper systems to achieve stringent technological requirements [12–15]. Microgripper mechanism can be fabricated by utilizing MEMS technology and/or conventional precision machining technology [4]. Regarding the materials used, silicon and metal materials were employed widely for compliant micromechanism. However, due to the advance of polymer technology, the trend in using polymer to fabricate microgripper has been progressively increasing recently [11]. Actually, the realization of microgripper by employing polymer is most important in considering its practical applications. A polymer microgripper is cost-effective, reliable, easily fabricated, and mostly, fit to biomedical manipulations.

The research and development of microgripper systems has attracted numerous mechatronic engineers for over 25 years. However, in reviewing the implemented microgripper systems [13, 19], it is noted that most prototypes were developed without treating them as technological products through mechatronic approach [3], not even to mention micromechatronic method. By recognizing a microgripper system as a micromechatronic system, instead of MEMS, it will allow for its differentiation as an identifiable class of engineering products which promotes the development of micromechatronic engineering.

In this chapter, a micromechatronic gripper system with mechanism made of polymer and driven by shape memory alloy (SMA) actuator is designed, fabricated, and tested. In the first part, implementation Axioms, which are originally employed for precision design, are proposed for the development of micromechatronic systems. System design and implementation guided by realization Axioms from conceptual design, preliminary design and manufacturing consideration, as well as detail design and manufacturing procedure is described. The next part of this chapter concerns the synergetic operation of the mechatronic gripper system. The

http://dx.doi.org/10.5772/67266

servo control of SMA driven microgripper is described. The applications of the microgripper system are tested. Finally, the mechatronic design and implementation of the microgripper system is concluded.

2. Realization axioms for micromechatronic systems

The realization axioms, which are originally proposed by Suh in system design [20], are extended for the development of a micromechatronic system. For effective realization of micromechatronic systems, the process is guided by two realization axioms in the mappings from functional requirements (FRs) to design parameters (DPs) and then from DPs to process variables (PVs). The two realization axioms are stated as follows [21, 22]:

Axiom 1. Functional independence

An optimal design of a micromechatronic system must maintain the independence of functional requirements of the mechatronic subsystems—mechanism, sensor, actuator, and controller.

Axiom 2. Information minimization

The best design of a micromechatronic system is a design of functionally independent subsystems with the minimum information content. Here, the information content is a measure of uncertainties in physical realization of the design specifications of a system and its subsystems.

As an example of micromechatronic systems, a microgripper system is to be realized under the guidance of realization axioms. By employing the axiom of functional independence, a microgripper system can be designed and realized with the merits of the independent module design, independent functional testing, and sufficient degrees of freedom in system implementation. With the axiom of information minimization in the processes of design, assembly, and manufacturing, a microgripper system can be realized, and it is expected to satisfy the stringent requirements such as micron accuracy, clean operation, and low cost. The synergetic operation of a mechatronic microgripper system is finally achieved by implementing optimal control software.

3. Conceptual design

3.1. Design objective and constraints

In the area of micromanipulation, there are numerous functional principles which can be applied for the manipulation of microobjects [13, 14, 19, 23, 24]. In the present design, the objective is to develop a reliable mechanical microgripper employed in biomedical industries for repetitive grasping and transporting microobjects. The requirements of no lubrication and no wear are essential for clean room operations. The objects are microhard particles with diameter around 20–40 μm. The operation is to be carried out in room temperature around

25°C. Under the constraints of limited working space, the cross-sectional size of microgripper system is to be less than $(\pi/4) \times 1^2$ mm^2.

3.2. Design mappings

A conceptual design on the micromanipulation system is described through design mappings between different domains. With the established design mappings, the optimal structure of the micromanipulation system can be implemented by following the realization axioms. The relationship between the highest *FR*s and the highest level *DP*s is first established. The highest *FR*s of the manipulation system is identified as three independent functions: *FR*1 = gripping and releasing of microparticle, *FR*2 = carrying gripper and particle in microoperation, and *FR*3 = acquiring working states in micromanipulation. The corresponding *DP*s of the micromanipulation system is identified as *DP*1 = microgripper system, *DP*2 = working stages, and *DP*3 = visual system. The design mapping between the *FR*s and *DP*s in the first level can be formulated as Eq. (1):

$$\begin{bmatrix} FR1 \\ FR2 \\ FR3 \end{bmatrix} = \begin{bmatrix} a_{11} & 0 & 0 \\ a_{21} & a_{22} & 0 \\ a_{31} & a_{32} & a_{33} \end{bmatrix} \begin{bmatrix} DP1 \\ DP2 \\ DP3 \end{bmatrix}, \tag{1}$$

where the matrix by $[a_{ij}]$ is to be characterized in the realization of the micromanipulation system. The mapping between *FR*s and *DP*s in Eq. (1) satisfies a decoupled module design of microgripper system, working stages, and visual system. By following the axiom of functional independence, the design mapping between the *FR*s and *DP*s can be realized by utilizing mechanism, sensor, actuator, and controller. For the development of a micromanipulation system, the design procedure can be obtained from Eq. (1). The mapping between *FR*s and *DP*s in Eq. (1) can be realized by starting from a_{11}. From the mapping by a_{11}, the microgripper system will be first realized. With the microgripper system and a_{21}, the a_{22} is obtained by realizing working stages to satisfy the functional requirement. With the mapping set up by a_{11}, a_{21}, a_{22}, a_{31}, and a_{32}, the a_{33} is obtained finally by realizing visual system to satisfy the functional requirement. As a result, the design procedure is given by the sequence: *FR*1 → *DP*1 → *FR*2 → *DP*2 → *FR*3 → *DP*3.

The microgripper system is the first subsystem to be realized for gripping and releasing microobject. The most essential hardware of microgripper system consists of microgripper mechanism (*DP*1.1) and microactuator (*DP*1.2). By following the Axiom 1, the microgripper mechanism and microactuator will be realized independently. Regarding the gripping and releasing function, the operation is realized by an end effector through gripper mechanism. The mapping between the execution of actuation to output motion (*FR*1.1) and the correspondent design parameters of microgripper mechanism (*DP*1.1) is further decoupled. By identifying *FR*1.1.1 = open/close gripper jaws, *FR*1.1.2 = fit microparticle, and *FR*1.1.3 = provide stable gripping and holding force as well as the corresponding *DP*1.1.1 = input to output mechanism, *DP*1.1.2 = openings and geometrical shape of gripper jaws, and *DP*1.1.3 = gripping point and contact surface, the mapping yields:

http://dx.doi.org/10.5772/67266

$$\begin{bmatrix} FR1.1.1 \\ FR1.1.2 \\ FR1.1.3 \end{bmatrix} = \begin{bmatrix} b_{11} & 0 & 0 \\ b_{21} & b_{22} & 0 \\ b_{31} & b_{32} & b_{33} \end{bmatrix} \begin{bmatrix} DP1.1.1 \\ DP1.1.2 \\ DP1.1.3 \end{bmatrix}. \tag{2}$$

The $[b_{ij}]$ in Eq. (2) is to be characterized by the realization of the conceptual design of microgripper mechanism as illustrated in **Figure 1**. Eq. (2) reveals that the achievement of stable gripping and holding object is relied on the design parameters: (1) input to output mechanism, (2) openings and geometrical shape of gripper jaws, and (3) gripping point and contact surface. In the realization of microgripper mechanism, the *DP*1.1.1 should be first implemented.

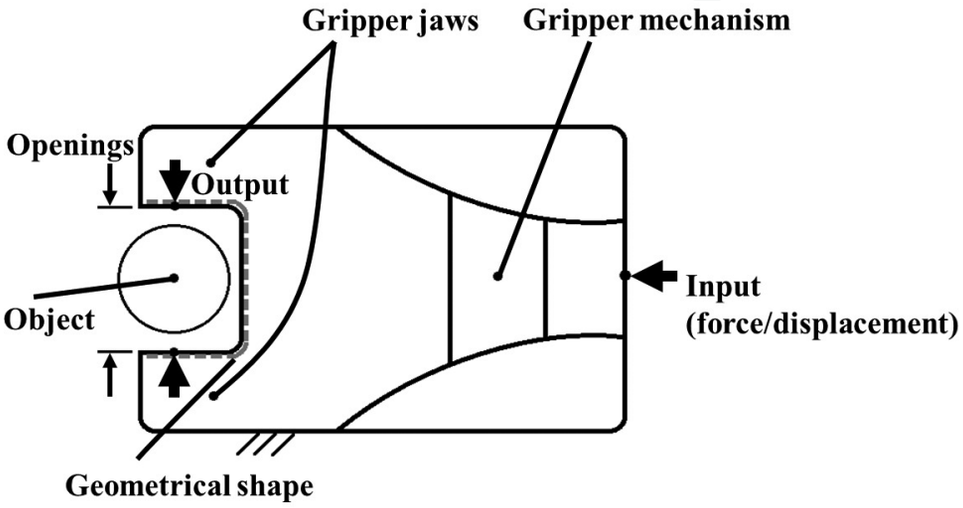

Figure 1. Conceptual design of microgripper mechanism.

From the requirement of design objective, the constraints of *DP*s in the design of microgripper system can be identified as: *DP1*–C_1 = clean operation, *DP*1–C_2 = accurate dimension, *DP*1–C_3 = micron repetitive operations, and *DP*1–C_4 = microgeometrical size. In the process domain, the corresponding *PV*s are stated as: *PV*1–C_1 = material selection, *PV*1–C_2 = fabrication method, *PV*1–C_3 = components configuration, and *PV*1–C_4 = assembly works. The functional mapping between the constraints of *DP*s and *PV*s can be formulated as Eq. (3):

$$\begin{bmatrix} DP1\text{–}C_1 \\ DP1\text{–}C_2 \\ DP1\text{–}C_3 \\ DP1\text{–}C_4 \end{bmatrix} = [c_{ij}] \begin{bmatrix} PV1\text{–}C_1 \\ PV1\text{–}C_2 \\ PV1\text{–}C_3 \\ PV1\text{–}C_4 \end{bmatrix}. \tag{3}$$

The $[c_{ij}]$ in Eq. (3) in general is not independent and the constraints are to be considered in the physical realization of microgripper mechanism and microactuator. In the process of realizing microgripper mechanism (*DP*1.1) or microactuator (*DP*1.2), the material selection, fabrication method, components configuration, and assembly works are crossly related. In the prototype development, the constraints on a microgripper mechanism are applied to its subsystems of end effector, transmission mechanism, and suspension frame. The constraints on a microactuator are

applied to its subsystems of actuating units, transmission mechanism, and structural frame. The constraints of components configuration and assembly works are applied to both microgripper mechanism and microactuator in the final assembly.

According to Eqs. (2) and (3), further detailed considerations in the conceptual design of the gripper mechanism are described. The Axiom 2 is employed for the design of a microgripper mechanism. For the minimization of information content, a mechanism is to be designed with simple configuration, symmetry, low number of links, and easy assembly. In considering the microgripper mechanism to be operated in a clean room, a one-piece compliant gripper, without assembly works, is selected and designed to provide accurate tip motion and proper gripping force. Since the microgripper mechanism needs to be reliable in micron-repetitive operations, an elastic material is selected to avoid fatigue in operations [18]. For providing a stable gripping of hard object, elastic contact gripping surfaces are used. Thus, without employing difficult surface treatment on microscale gripper surface, polymer elastomer will be considered for fabricating the gripper mechanism. For achieving the accurate and precise fabrication of microgripper mechanism, a lithography method through mask will be selected.

For accurate driving a microgripper, a microactuator which can provide micron operation with high actuating force is to be realized. At first, it is observed that SMA actuator is relatively small compared with other type of actuators under the same driving energy and output stroke [25]. If one considers the requirements to fit different applications, it is noted that the operational characteristics as well as geometrical shape and size of SMA can be conveniently designed and fabricated. A concern in fabricating SMA actuator is the constraint of geometrical size. Since a biased spring is required to overcome martensite twinning for the recovery of the initial shape in a fast two-way operation, the assembly works of SMA and biased spring make it difficult or even impossible to achieve microsize. Thus, by following the Axiom 2 and under the guidance of Eq. (3) in the realization of SMA actuator, an innovative design of SMA actuator without encountering the assembly issue is to be developed.

In order to focus on the present implementation of microgripper system, an industrial micromanipulation platform will be selected for realizing the working stages (*DP*2) and visual system (*DP*3). The selection of micromanipulation platform is guided by the Axioms 1 and 2. The visual system to be selected is to consider the specifications of constituent components: image card, image processing algorithm, microscope, illumination light, and CCD subsystem. In the selection of working stages for installing the microgripper system, one needs to consider working stroke, accuracy, speed, and degrees of freedom.

For the synergetic operation of the micromanipulation system, the control system consists of hardware and software. The electrical control hardware includes signal conversion, signal detection, impedance matching, and power amplification. The control hardware can be implemented by employing analogue and/or digital circuit elements. The controller includes cascade compensator, feed forward, and feedback control. For the operation of contact avoidance, gripping, releasing, and holding, the control signal can be implemented by employing software and running on a personal computer.

http://dx.doi.org/10.5772/67266

4. Preliminary design and manufacturing consideration

4.1. Gripper mechanism

Polymer elastomer is a viscoelastic material with the nonlinear and time-varying stress-strain behaviors: precondition, creep deformation, stress relaxation, and hysteresis [26]. These behaviors shown in a compliant mechanism depend on the amount of the distributed material which mainly contributes to deflected compliant motion. If the distributed material is lumped in the compliant joint, the amount of the deformed material will be the minimum and consequently, the nonlinear and time-varying effect will reduce. Thus, when the compliant-joint mechanism is operated under temperature and humidity-controlled environment, the small-deflected motion can be properly described through a linear time-invariant system which facilitates accurate motion control. As a result, a lumped-compliant-joint instead of distributed-compliant gripper mechanism is selected for achieving simplified model and accurate motion control. In designing a gripper with lumped-compliant joints, at first, one needs to select a topological linkages model for the kinematic structure of mechanism. Then the correspondent compliant structure will be transformed into a pseudo linkages model (PLM) with equivalent lumped springs [21, 26]. Finally, the compliant mechanism of the PLM is synthesized under the constraints of kinematics, material, and fabrication. In the preliminary consideration, it is expected to scale down the mechanism of a mesoscale compliant gripper which had been implemented [21]. The mesoscale compliant gripper, in which the topological structure was selected from the existing types of conventional mechanism, was a design with six links and six joints and manufactured by employing elastomer. When the gripper mechanism is scaled down to microsize; however, the stiffness of compliant joints in polymer gripper will greatly decrease. As a result, the downscaling microgripper with low input-output stiffness will cause high positioning errors in gripping operations.

For the improvement of the input-output stiffness, the modification or reconstruction of PLM is required in downscaling the mesoscale polymer gripper. It is noted that the compliant gripper is a structure with compliance lumped in its joints. The compliant joint actually will deform in several degrees of freedom when it is subjected to complex load in operations. Thus, the planner motion of compliant joint in a gripper will have both angular and linear deflections when external force and/or moment are applied. The existence of deflection other than angular deflected motion is most severe when the compliant joint is manufactured by utilizing elastomer. Considering the deflections of a right circular joint with radius r, minimum width of joint t, and thickness h as illustrated in **Figure 2**, the formulas of Paros and Weisbord [27] can be utilized for deflection analysis. For a right circular joint with $\frac{r}{t} \geq 2$ and with linear elastic material properties: Young's modulus E, Shear modulus G, and Poisson's ratio ν, the angular and shear stiffness of the joint can be expressed, respectively, as

$$K_\theta = \frac{M_z}{\Delta\theta} \approx \frac{2Ebt^{2.5}}{9\pi r^{0.5}}, \tag{4}$$

$$K_s = \frac{F_y}{\Delta s} \approx \frac{Gb}{(-2.57 + \pi(r/t)^{0.5})}. \tag{5}$$

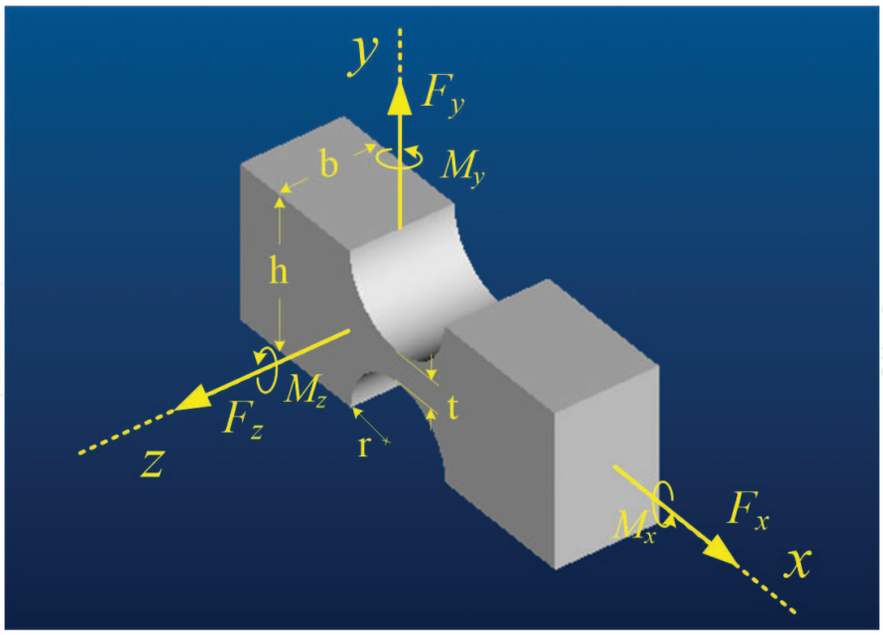

Figure 2. Geometrical dimensions and loadings of a right circular joint.

From Eqs. (4) and (5), it is observed that the relative magnitude between angular and shear deformations of a compliant joint mainly depends on the *r*/*t* ratio and material properties in design. If the geometrical size is fixed, the joint stiffness by Eqs. (4) and (5) will only depend on the material properties. Since the shear modulus of elastomer is relatively small, the deformation in the compliant joint by Eq. (5) needs to be included in a PLM model to account for the degrees of freedom in sliding. The sliding motion in the compliant joint will reduce the input-output stiffness of the downscaling mesoscale polymer gripper. In order to increase the input-output stiffness, a direct solution is to reduce the numbers of compliant joints in the gripper mechanism. By reducing the degrees of freedom of the mesoscale gripper in downscaling through eliminating two symmetric outer joints in the gripper, an equivalent PLM with one degree of freedom in kinematics is finally constructed as shown in **Figure 3**. For the compliant gripper mechanism, the PLM is identified as a mechanism with six linkages, four joints, and three sliders.

4.2. SMA actuator

An innovative SMA actuator to overcome the assembly issue is to be developed. The innovative design is to consider a self-biased SMA (SB-SMA) actuator without employing biased spring. A SB-SMA actuator can be implemented to include the effect of biased-spring in the fabrication of SMA microactuator through introducing prestrain in the SMA material. A novel SB-SMA actuator has been developed and employed for actuating microgripper in gripping and assembly applications [12]. The advantage of heating prestrained SMA wire in closing operation was investigated recently [28]. The implementation of the SB-SMA actuator will be described in the detail design and manufacturing procedure.

http://dx.doi.org/10.5772/67266

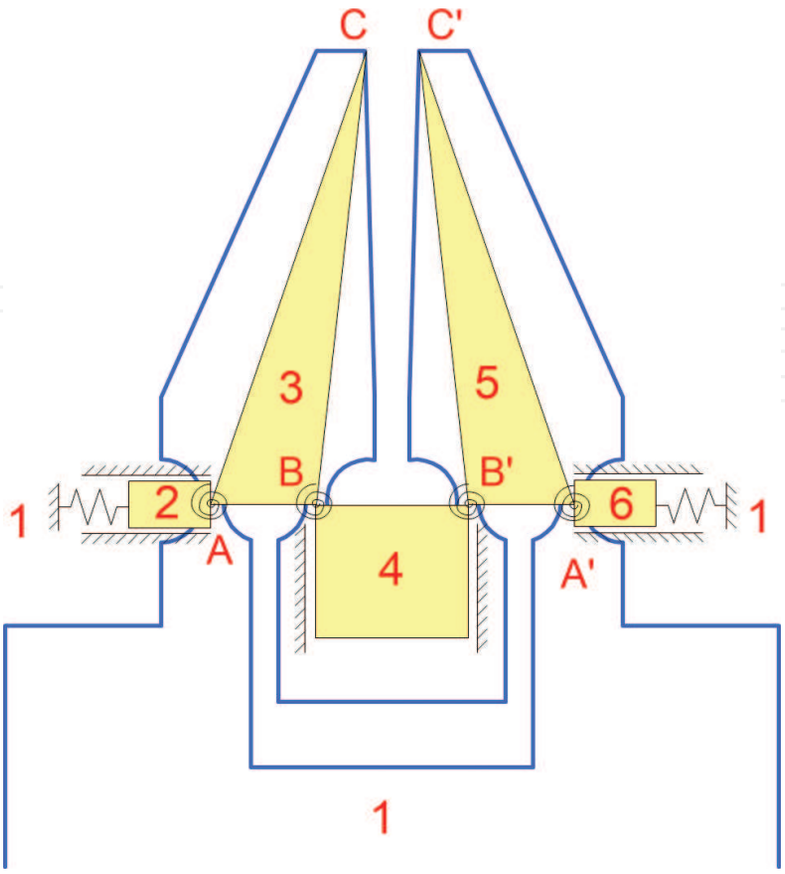

Figure 3. Preliminary design of microgripper mechanism and its PLM.

5. Detail design and manufacturing procedure

5.1. Gripper mechanism

In this phase, it is to synthesize an optimal shape and size of the compliant gripper mechanism. Under the design constraint of 1 mm width for the microgripper mechanism, an optimal PLM of gripper is obtained for the objective: amplifying the input displacement to output displacement and achieving the operation of parallel gripping.

The microgripper mechanism and its PLM are shown in **Figure 3**. In **Figure 3**, the contour line shows a geometrical shape of the gripper mechanism and its structural frame. The PLM is modeled as a six-linkage mechanism for providing one degree of freedom in input-output motion. When an actuating force *F* as input is applied, the actuator will drive link 4 to produce output displacement. Due to the constraints of structural frame 1, both links 3 and 5 will rotate and translate to cause the gripping operation by tips *C* and *C′*.

Regarding the PLM, the motion kinematics will be analyzed. In the following derivation, the assumption of small deformation is used. In the kinematic analysis, the two gripper arms are assumed to be driven simultaneously by a vertical sliding mechanism in gripping operation. In considering the output at gripping point *E*, which is closing to *C*, the kinematic motion of the

left gripper arm of PLM is depicted as shown in **Figure 4**. From **Figure 3** and **4**, the horizontal and vertical displacement gains can be derived as the ratio between the gripping point displacement Δx, Δy, and input displacement Δi of slider 4, respectively, as

$$G_x = \frac{\Delta x}{\Delta i} = \frac{L_2 \cos \beta}{L_1}, \tag{6}$$

and

$$G_y = \frac{\Delta y}{\Delta i} = \frac{L_2 \sin \beta}{L_1}, \tag{7}$$

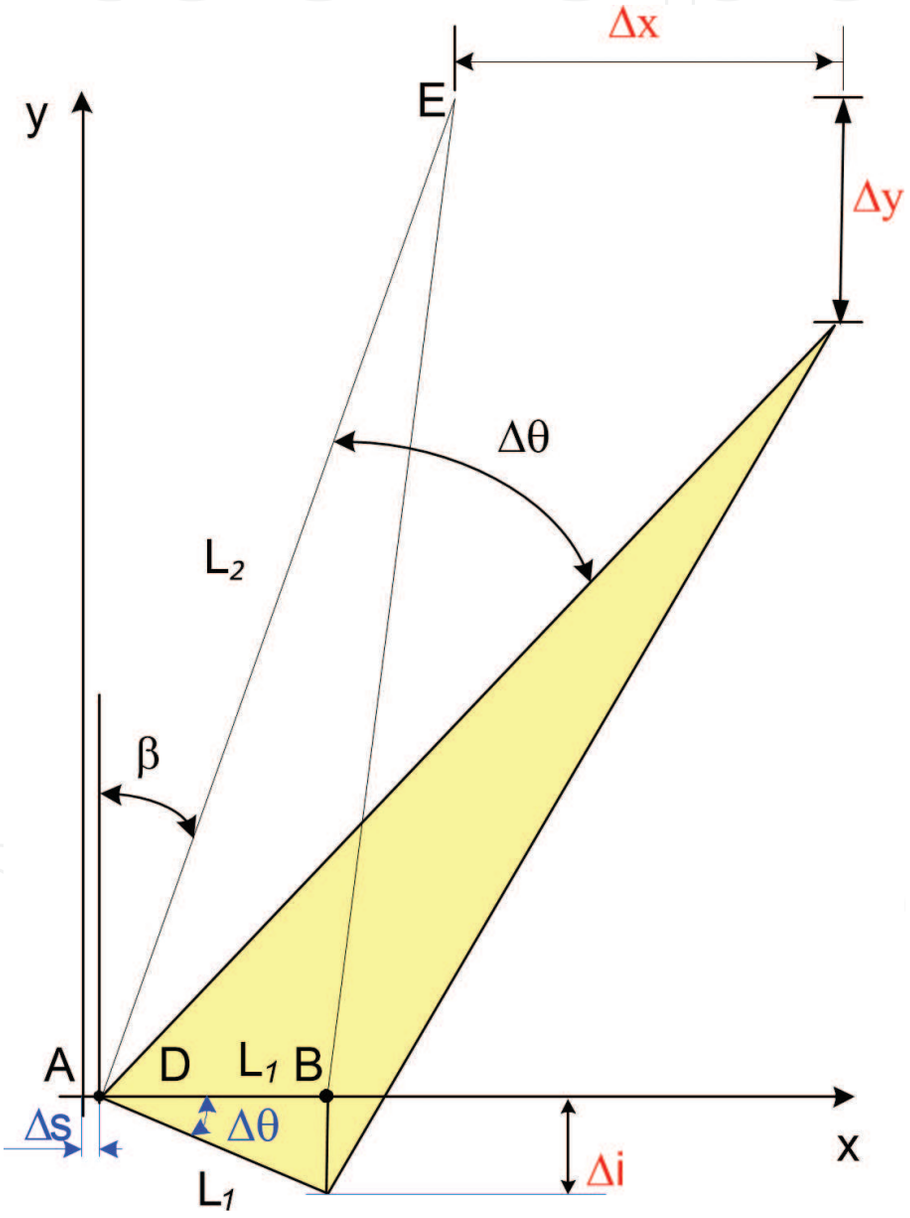

Figure 4. Kinematic motion relation of PLM in **Figure 3.**

where $L_1 = \overline{AB}$, $L_2 = \overline{AE}$, and β is the angle between a vertical line and $\overline{AE}$. For achieving parallel gripping, it is expected that $G_x \gg G_y$.The horizontal displacement of gripper tip can be expressed:

http://dx.doi.org/10.5772/67266

$$\Delta x = G_x L_1 \sin\Delta\theta. \tag{8}$$

In the synthesis of compliant gripper for accurate operation, it is noted that finite element analysis, kinematic PLM, and experimental test needs to be utilized closely together [26]. The detail geometry and size of the compliant microgripper is finally determined under the constraints of manufacturing technologies, stiffness of compliant joint, and availability of polymer material. The material of thermoplastic polyurethane (PU) film is selected from local industry. The material properties are given in **Table 1**. The r/t of the designed compliant joint is about 2.0. The size of microgripper mechanism was designed as 937 μm × 477 μm. The kinematic design gave G_x = 4.1, G_y = 1.5 by employing ANSYS analysis. The microgripper was manufactured by utilizing Excimer Laser, Exitech 2000, with mask projection through 10x size reduction by an optical lens. The final product of PU gripper mechanism was shown in **Figure 5**.

PU film	Thickness	100 μm
	Young's modulus	76.4 MPa
	Poisson's ratio	0.47
	Melting point	200°C
SMA wire	Alloy	NiTi
	Austenite starting temperature	70°C
	Diameter	38 μm
	Resistance	0.89Ω/mm

Table 1. Materials for designing gripper mechanism and actuator (@ temperature 24–26°C, humidity 40–44%).

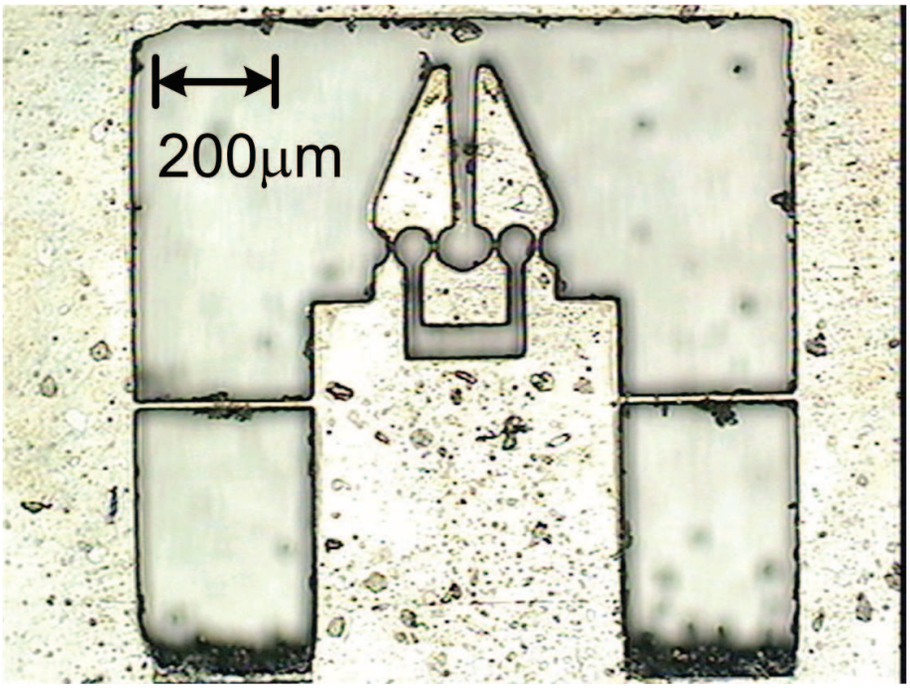

Figure 5. Final product of microgripper mechanism.

5.2. SB-SMA actuator

For manufacturing SB-SMA actuator, a roll of SMA wire was first obtained from Dynalloy, Inc. The material properties are given in **Table 1**. The SMA wire was cut to provide a 2 mm working length plus margin length on two ends for wiring. The wiring of the SMA actuator with copper wire was realized by utilizing silver glue. Two nonconductive glass plates of 1 μm thickness were used for the frame. The SMA wire was finally bent into an arc shape and glued together for introducing prestrain in the wire as shown in **Figure 6**. The heating and cooling of the SB-SMA in operation was undertaken, respectively through electrical resistance and still air. The still air was maintained at 24–26°C. In experimental test, the tip position of SB-SMA actuator was measured by utilizing a microscopic computer-vision system through correlation method [11]. The resolution of the image system was adjusted and calibrated to give 1.26 μm/pixel. A correlation method with further data processing was employed for finding the tip position of SB-SMA. For the microactuator, it provided 5 μm stroke with input 50 mA under 3 V.

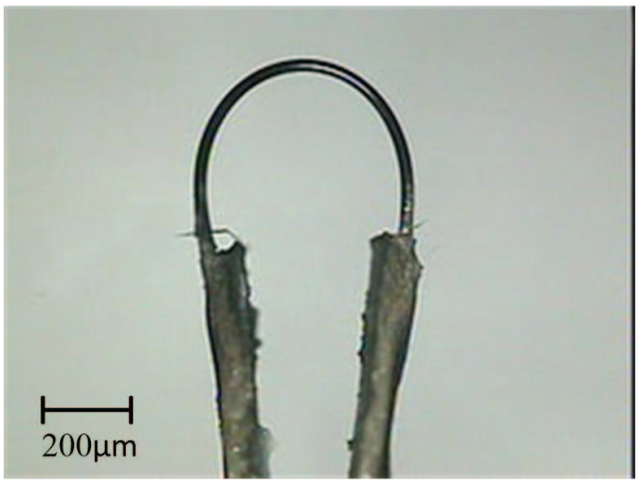

Figure 6. Final product of arc-shape SB-SMA actuator.

5.3. Assembly and test of microgripper system

The gripper system was assembled by the functional independent gripper mechanism and actuator. The assembled configuration of the planner gripper mechanism and actuator was to be perpendicular. The assembly procedure was to insert the SB-SMA actuator to the actuated point, then rotated it to the base, and finally did fine tuning and glued together [12]. For assuring a tight contact between the actuator and gripper in operation, a mechatronic approach, instead of moving and adjusting contact point [11], by applying a small biased-current to SMA in operation was preferred. After assembly, the cross-sectional area of the microgripper system was about $(\pi/4) \times 500^2$ μm^2. The testing of microgripper system was undertaken by the experimental setup with working stages and visual system as given in the installation [11]. When an electric current of 70 mA at 3 V was applied, the gripper was almost fully closed. By employing the realization Axioms, a micromechatronic gripper system was effectively implemented to satisfy design constraints at less repetitively corrective processes.

http://dx.doi.org/10.5772/67266

6. Servo control of SB-SMA drive microgripper

6.1. Measurement of the first-order descending curves

The Preisach model of SMA is constructed as a model consisting of many nonideal relays connected in parallel, given weights, and summed for the hysteresis behaviour. The model between input *u(t)* and output *y(t)* is expressed as [25, 29]

$$y(t) = \iint_{\alpha \geq \beta} \mu(\alpha, \beta) \gamma_{\alpha\beta}\Big(u\ (t)\Big) d\alpha d\beta, \tag{9}$$

where $\gamma_{\alpha\beta}$ are hysteresis operators for nonideal relays, α and β are the increasing and decreasing thresholds, respectively, and $\mu(\alpha, \beta)$ are Preisach functions.

The Preisach model from input current to output displacement is implemented numerically. Along with the input history *u(t)*, a sweeping region is expressed in the Preisach plane. The output change along the descending branch from α_i to β_j is defined as

$$Y(\alpha_i, \beta_j) = y_{\alpha_i} - y_{\alpha_i \beta_j}, \tag{10}$$

where y_{α_i} is the output displacement at input current value of α_i and $y_{\alpha_i \beta_j}$ is the output displacement after the current has been decreased to β_j from its maximum value of α_i. By dividing the sweeping region for calculating the output into *n(t)* trapezoids along with $Y(\alpha_i, \beta_j)$, the output change along the descending branch from α_i to β_j can be calculated. The output displacement by Preisach hysteresis can be calculated by utilizing the first-order descending (FOD) surface. By expressing the area of each trapezoid in Preisach plane as a difference between two triangle areas, the output displacement is derived by adding and/or subtracting all $Y(\alpha_i, \beta_j)$ with the corresponding triangular areas of edge (α_i, β_j). In the consideration of increasing or decreasing input *u(t)*, the output displacement is derived:

For $\dot{u}(t) \leq 0$,

$$y(t) = \sum_{k=1}^{n(t)-1} [Y(\alpha_k, \beta_{k-1}) - Y(\alpha_k, \beta_k)] + \left[Y\Big(\alpha_{n(t)}, \beta_{n(t)-1}\Big) - Y\Big(\alpha_{n(t)}, u(t)\Big)\right], \tag{11}$$

For $\dot{u}(t) > 0$,

$$y(t) = \sum_{k=1}^{n(t)-1} [Y(\alpha_k, \beta_{k-1}) - Y(\alpha_k, \beta_k)] + Y\Big(u(t), \beta_{n(t)-1}\Big). \tag{12}$$

The detail description about the experimental collection of data for FOD curves is referred to [29]. From experimental tests and with data processing, a set of FOD curves was processed, and finally depicted in **Figure 7**.

6.2. Inverse Preisach compensation

For compensating the nonlinear SB-SMA actuator accurately, the strategy is to cascade an analytical inverse Preisach model. The inverse of Preisach model, that determines the current

resulting in a desired displacement, is derived from Eqs. (11) and (12). The feed forward inverse compensator u_{Ff} for the desired output displacement $y_d(t)$ is implemented through the inverse function of Y as Y^{-1} and given by [30]:

For $\dot{u}(t) \leq 0$,

$$u_{Ff}(t) = Y_{\beta}^{-1}[\alpha_{n(t)}, \sum_{k=1}^{n(t)-1}[Y(\alpha_k, \beta_{k-1}) - Y(\alpha_k, \beta_k)] + Y(\alpha_{n(t)}, \beta_{n(t)-1}) - y_d(t), \tag{13}$$

For $\dot{u}(t) > 0$,

$$u_{Ff}(t) = Y_{\alpha}^{-1}[y_d(t) - \sum_{k=1}^{n(t)-1}[Y(\alpha_k, \beta_{k-1}) - Y(\alpha_k, \beta_k)], \beta_{n(t)-1}]. \tag{14}$$

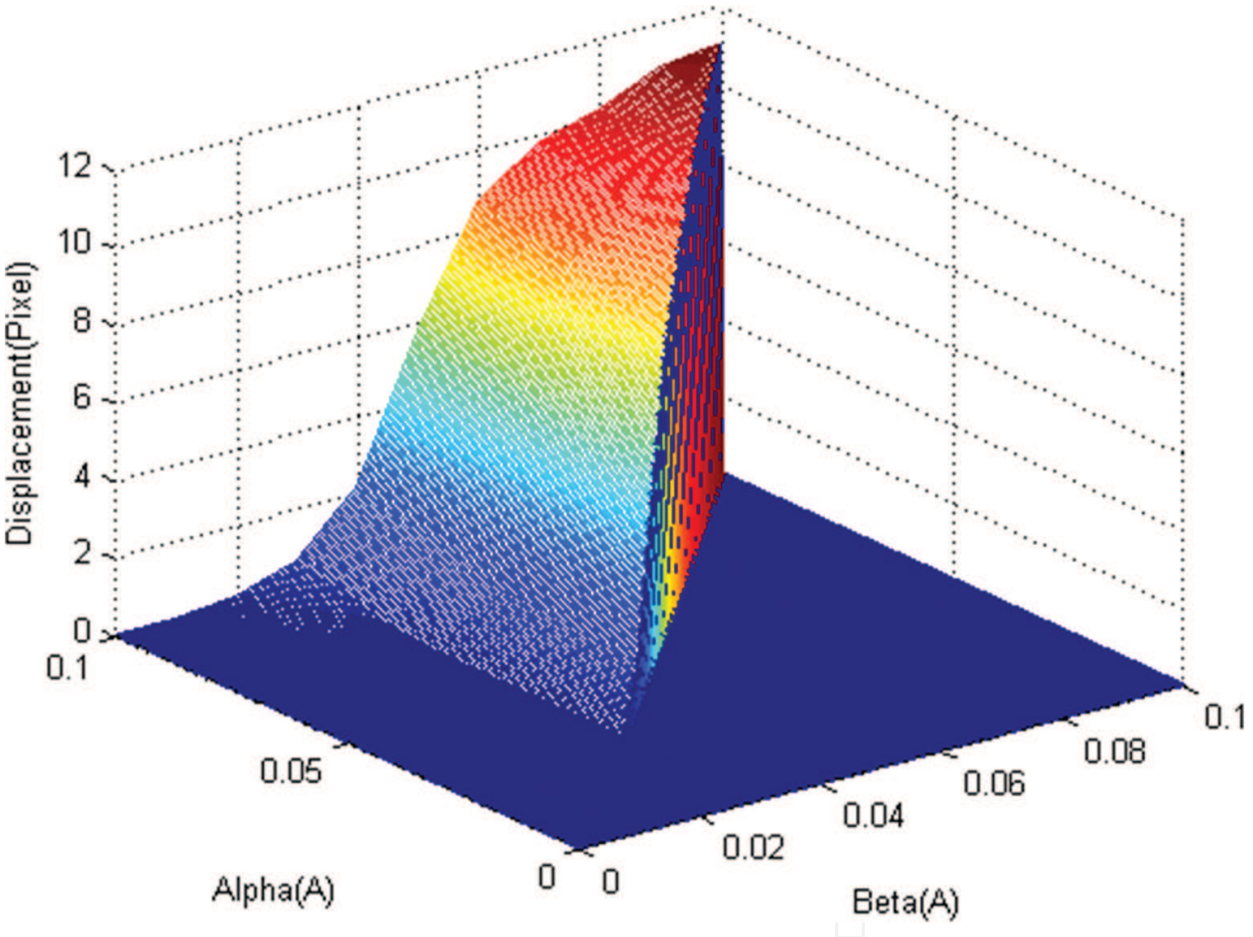

Figure 7. FOD surface of SMA.

In motion control, the SB-SMA microactuator was operated dynamically in the phase transformation during the heating and cooling processes. In experiment, the sampling frequency was 30 Hz. For investigating the dynamic behaviour of the SB-SMA actuator under analytical inverse Preisach compensation, sinusoidal input tests were undertaken. Experimental results revealed that the output displacement was highly fluctuated, especially when the SB-SMA actuator was operated to reverse its motion direction. For obtaining reliable measurement of actuator displacement by the correlation method, a low-pass filter was cascaded. Since the

bandwidth of SB-SMA actuator was less than 5 Hz, in considering the response speed of the SB-SMA actuator, a 3rd-order Butterworth filter $G_f(z)$ with 5 Hz cutoff frequency was implemented:

$$G_f(z) = \frac{0.049z^3 + 0.149z^2 + 0.149z^1 + 0.049}{z^3 - 1.162z^2 + 0.695z^1 - 0.138}. \tag{15}$$

The sinusoidal displacement response of the compensated SB-SMA under the two different input amplitudes was recorded, as shown in **Figure 8**. From the experimental results of sinusoidal input of 0.025 Hz, it was observed that the output response followed the input command after short-time transient but the error in amplitude increased as the input amplitude increased.

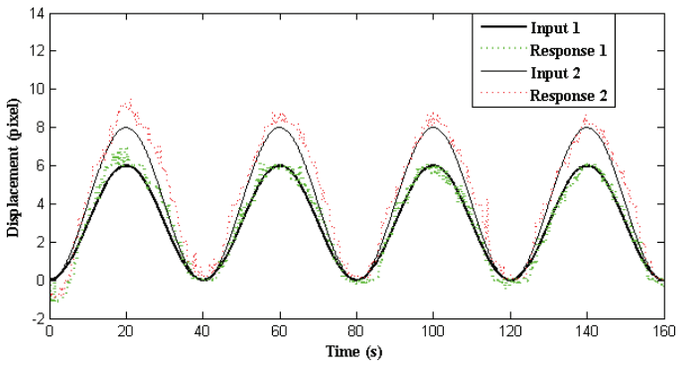

Figure 8. Sinusoidal test of SB-SMA actuator with inverse Preisach compensator.

6.3. Visual servo of microactuator

In controlling SMA actuator, the thermal and stress-dependent hysteresis behavior in phase transformation makes accurate control difficult. For the SB-SMA microactuator, the dynamic behaviour is even rather time-varying and consequently, it is difficult to achieve accurate offline compensation. A control strategy involving online identification is preferred for tracking the dynamics of SB-SMA actuator. An explicit self-tuning controller through the Ziegler-Nichols criterion [31] is selected for controlling the Preisach compensated SB-SMA actuator.

In an ideal Preisach compensated SB-SMA actuator, the dynamic model can be described as a linear time-varying system. By assuming that the SB-SMA actuator is a second-order system, the model can be described by

$$y(k) = \Theta^T(k)\Phi(k-1) + e(k). \tag{16}$$

The parameter vector and state vector, respectively in Eq. (16) is given as

$$\Phi(k-1) = [y(k-1), y(k-2), u(k-1), u(k-2)], \tag{17}$$

$$\Theta(k) = [a_1, a_2, b_1, b_2]. \tag{18}$$

By employing a recursive identification algorithm from Matlab, the parameter vector of system, Eq. (18), can be estimated to give $\hat{\Theta}(k) = [\hat{a}_1, \hat{a}_2, \hat{b}_1, \hat{b}_2]$ [32]. Considering the SB-SMA

actuator is operated with proportional control gain k_p and in a unity feedback loop, the characteristic equation of the closed-loop system is obtained:

$$\Delta(z) = z^2 + bz + c = 0, \tag{19}$$

where $b = \hat{a}_1 + b_1 k_p, c = \hat{a}_2 + k_p \hat{b}_2$.

For a specific k_p, the feasible location of closed-loop poles to be located on unit circle can be classified according to the conditions: $b^2-4c > 0, b^2-4c = 0, b^2-4c < 0$. The three different cases are utilized to determine the critical gain k_{pu} and the associated critical oscillation frequency ω_k or period T_u for the feasible location of the closed-loop poles [31].

Based on the aforementioned three cases, the critical gain as well as critical oscillation period can be obtained and the control gain is derived by employing Ziegler-Nichols tuning rule. Regarding Ziegler-Nichols setting, $k_p = k_{pu}/2$ is for P control, $k_p = k_{pu}/2.2$, $k_i = 1.2k_{pu}/T_u$ is for PI control, and $k_p = 0.6k_{pu}$, $k_i = 2k_{pu}/T_u$, $k_d = k_{pu}T_u/8$ is for PID control. Thus, the PID controller with sampling time T_0 is implemented as

$$u(k) = k_p e(k) + k_i T_0 \sum_{i=1}^{k} e(i-1) + \left(\frac{k_d}{T_0}\right)[e(k)-e(k-1)]. \tag{20}$$

In practical control implementation, the control block diagram including inverse Preisach compensator, recursive least square estimator, PI tuning controller, visual position estimator, and low-pass filter for SB-SMA actuator is shown in **Figure 9**. In considering that the signal was highly fluctuated, only PI control in Eq. (20) was employed. In practice, the upper bound of k_i and k_p was limited to 2.5 to avoid excessive control input. The sampling frequency in the closed-loop system was 30 Hz. In each time step, the maximum value of the tuning gain was 0.3 to prevent the SMA vibration when system gain was changed. The low-pass filter was given by Eq. (15). The recursive least-square estimator was a forgetting factor algorithm with $\lambda = 0.98$ in Matlab function.

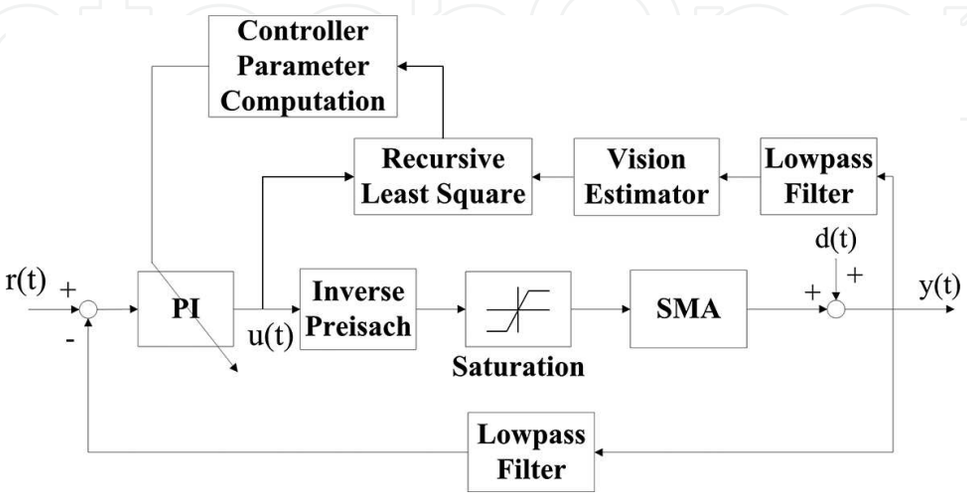

Figure 9. Control structure of self-tuning PI with inverse Preisach compensator.

For comparing the performance of the proposed controller, the fuzzy control schemes, which were usually utilized for system with uncertainty, with and without inverse Preisach compensator were also included. The block diagram of the fuzzy control schemes is shown in **Figure 10**. In the fuzzy control, the membership functions of error *e(t)*, error rate *de(t)*, and control input *u(t)*, were given as triangular functions. The expert knowledge by the fuzzy rules was given by the knowledge base as fuzzy sliding mode control. In fuzzy rules, the linguistic meaning of error *e* and error increment *de* are represented by utilizing symbol NB, NM, NS, ZE, PS, PM, and PB, respectively, for negative big, negative medium, negative small, zero, positive small, positive medium, and positive big. The knowledge base is shown in **Table 2**. For eliminating the steady-state error due to uncertain control bias, an integral control action with $k_i = 1.5$ was included. In the performance test, the system input was a multistep function. The experimental results of three control schemes were recorded, as shown in **Figure 11**. From the five consecutive steps, responses of **Figure 11**, the average rising time (0–100%), steady-state average absolute error, and average percentage overshoot were measured and calculated which are given in **Table 3**. According to the results listed in **Table 3**, the closed-loop performance of three different control schemes was compared. The results revealed that the inclusion of inverse Preisach compensator increased response accuracy but decreased response speed. The fuzzy control with I and without inverse Preisach gave the fastest response; however, it yielded the largest overshoot. The response speed by self-tuning PI with inverse Preisach was almost the same as that by fuzzy with I and inverse Preisach. Among the three control strategies, the self-tuning PI with inverse Preisach compensator achieved the best accuracy in both transient and stead-state responses.

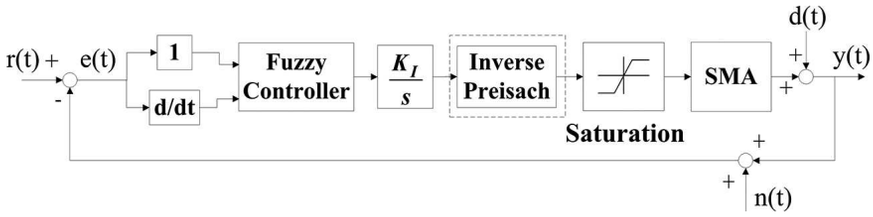

Figure 10. Structure of fuzzy control.

		Error						
		e						
Error rate		**NB**	**NM**	**NS**	**ZE**	**PS**	**PM**	**PB**
de	**PB**	ZE	PS	PM	PB	PB	PB	PB
	PM	NS	ZE	PS	PM	PB	PB	PB
	PS	NM	NS	ZE	PS	PM	PB	PB
	ZE	NB	NM	NS	ZE	PS	PM	PB
	NS	NB	NB	NM	NS	ZE	PS	PM
	NM	NB	NB	NB	NM	NS	ZE	PS
	NB	NB	NB	NB	NB	NM	NS	ZE

Table 2. Knowledge base of 49 fuzzy rules.

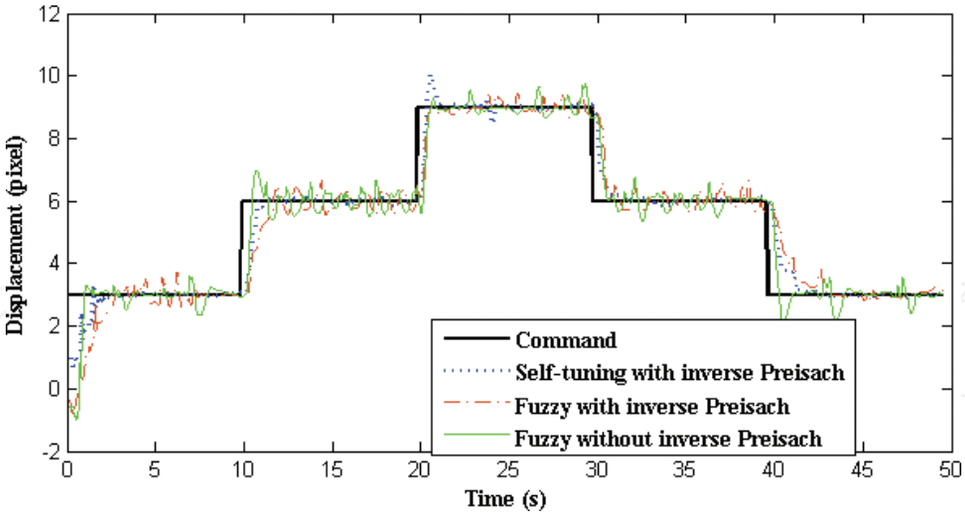

Figure 11. Multi-step input response by different control schemes.

Control method	Average rising time (s)	Steady-state average absolute error (pixel)	Average percentage overshoot (%)
Self-tuning PI with inverse Preisach	1.77	1.55	2.22
Fuzzy with I without inverse Preisach	0.64	5.72	11.26
Fuzzy with I and inverse Preisach	1.79	5.45	4.60

Table 3. System performance of three types of controller.

7. Microgripper applications

An experimental setup was installed for the testing of the gripping and transporting performance in controlling the microgripper system [11]. In the experimental tests, the measurement and testing was undertaken at room temperature 24–26°C and humidity 40–44%. The displacement measured by the image system was calibrated to give 1.26 μm/pixel. The present gripper was measured to give L_1 = 63 μm and G_x = 4.35. The G_x has an error of 5.75% in design.

In the gripping tests, a self-tuning PI with inverse Preisach control under visual servo was selected and employed for the closed-loop controller. The closed-loop block diagram is shown in **Figure 12**. In **Figure 12**, it was noted that a small backlash could be included to model the gap between the actuator driving point and the actuated point of microgripper. The backlash would be compensated by applying a small-biased current in operation.

The gripping test was undertaken by moving the microgripper to grip and transport a glass particle of 30 μm that was stick on the edge of a glass plate, as shown in **Figure 13**. After approaching the microparticle, the performance of controlling microgripper was to test its gripping operation. The input command to the gripper was to close 12 μm, i.e. 6 μm on each gripper jaw.

http://dx.doi.org/10.5772/67266

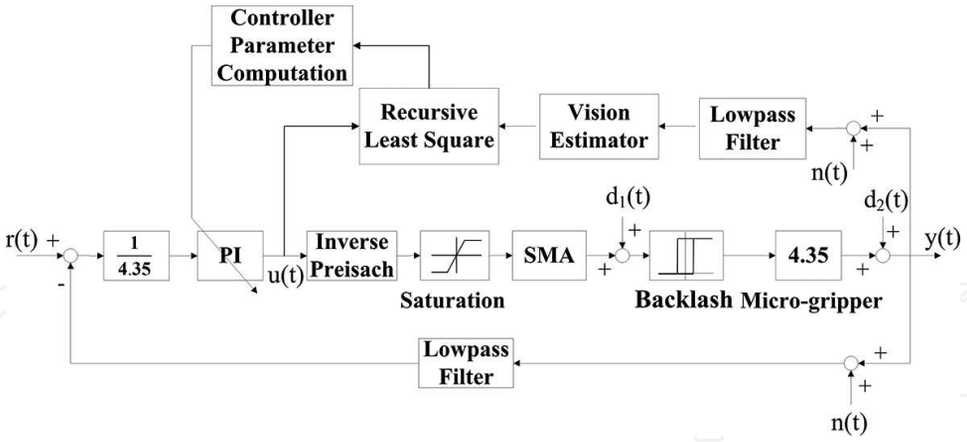

Figure 12. Block diagram of closed-loop control of SB-SMA actuated microgripper.

The displacement response of gripper jaw at one side was obtained by employing the kinematic relation of PLM together with measuring rotational angle of gripper jaw. As seen from **Figure 13(a)** and **Figure 13(b)** and employing regional scanning with edge fitting (RSEF) algorithm [7], the rotational angle $\Delta\theta$ was estimated and consequently, a one-sided horizontal displacement of gripper jaw was calculated by using Eq. (8).

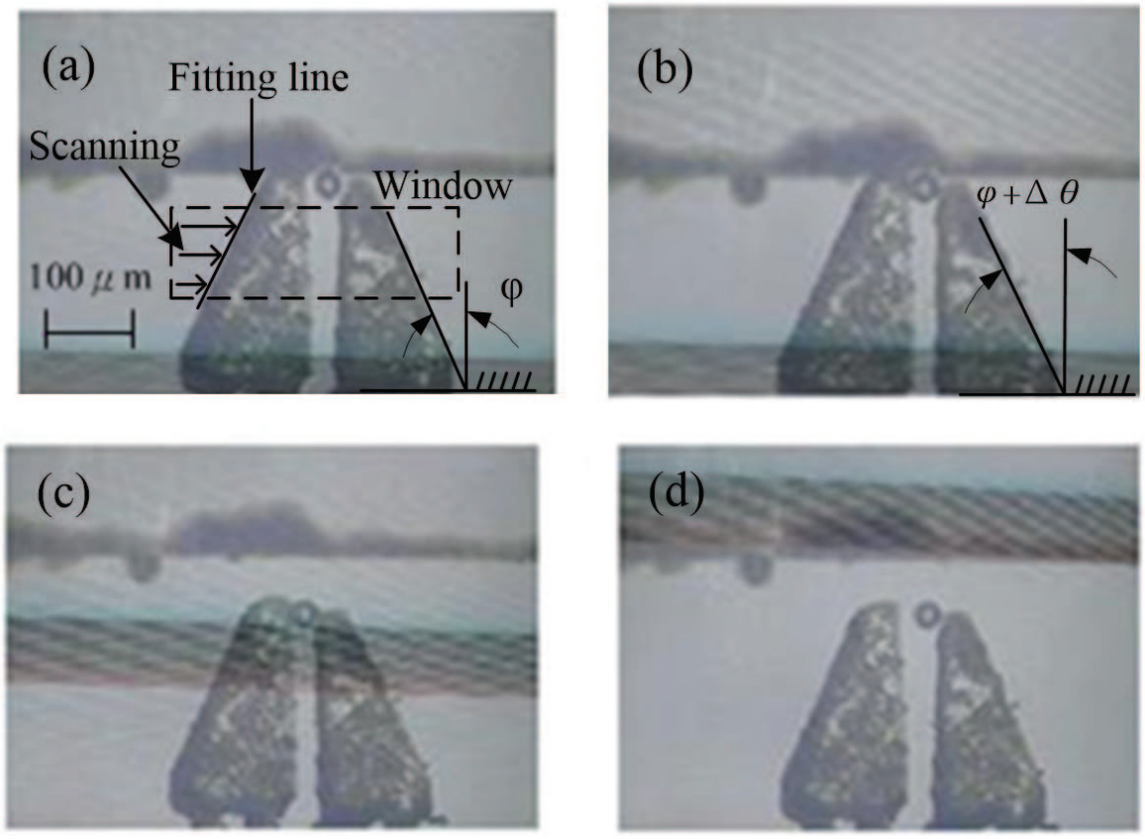

Figure 13. A microgripper is to approach (a), grasp (b), transport (c), and release (d) a 30 μm particle. The RSEF algorithm for measuring rotational angle is illustrated in (a) and (b).

For the input command of closing 12 μm, the command and gripping response of one-side jaw were recorded as shown in **Figure 14**. **Figure 14** revealed that the gripper jaw closed to almost

6 μm in 1.4 s and then decreased and oscillated until it was settled around 1 μm. In closing the gripper jaws, the first displacement peak was occurred when the gripper jaws touch and squeeze the microparticle. The contact and impact by microparticle caused highly fluctuated response in gripper jaw; however, the closed-loop controller effectively regulated the response to reach almost steady state at 4 s.

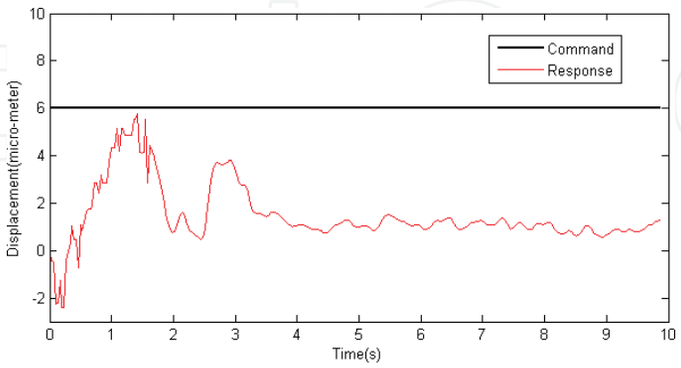

Figure 14. Response of one-side gripper jaw in gripping particle by self-tuning PI with inverse Preisach control.

The gripping operation was also utilized to estimate the particle size. The steady-state gripper closing without gripping particle was first tested and obtained. In steady state, the rotational angle was measured to give $\Delta\theta = 3.5°$ which leaded to a horizontal displacement of 16.73 μm. Consequently, without gripping particle, the horizontal displacement of gripper jaws was 33.46 μm. Considering the response in gripping particle as given by **Figure 14**, the steady-state displacement of gripper jaw was around 1 μm by one-side jaw, which was estimated as 2 μm by two-side jaws. Therefore, the size of microparticle was estimated to give 31.46 μm. The estimated error of particle size was 4.87%.

8. Conclusions

The realization axioms and design procedure are proposed for implementing micromechatronic systems. As an example of micromechatronic systems, a micromechatronic gripper was designed, fabricated, and tested with the visual-based control system. The microgripper system consisted of PU microgripper mechanism and SB-SMA actuator. By employing realization axioms, a micromechatronic gripper system was efficiently and effectively implemented to achieve high gripping performance at low cost expense. The micromechatronic gripper system was realizable with the cross-sectional area of $(\pi/4) \times 500^2$ μm^2 for clean room operation. A synergetic operation of SB-SMA actuator for driving microgripper mechanism was investigated in visual-based control. In the visual servo of SB-SMA actuator, a self-tuning PI with inverse Preisach compensator, as compared with fuzzy control schemes, gave the best accuracy in transient and steady-state responses. The micromechatronic gripper system was utilized to grasp and transport a glass particle of 30 μm. In the grasping test, the self-tuning PI with inverse Preisach compensator effectively regulated the closing response of gripper jaws in contact with glass particle. In addition, in holding the particle under visual servo, the size

of glass particle was estimated to give an error of 4.87%. The PU gripper system is cost effective to achieve high performance operation. For future sensitive biomedical field operations, the error by the prototype gripper needs to be further improved. In considering the manipulation of biological object, the gripper system needs to be tested in a liquid environment.

Acknowledgements

The authors would like to thank the Ministry of Science and Technology (MOST) for the partial support provided under contract No.105-2221-E-006-081.

Author details

Ren-Jung Chang* and Yu-Heng Lai

*Address all correspondence to: rjchang@mail.ncku.edu.tw

Department of Mechanical Engineering, National Cheng Kung University, Tainan, Taiwan, Republic of China

References

[1] Harshama F, Tomizuka M, Fukuda T. Mechatronics—what is it, why, and how? An editorial. IEEE/ASME Trans. Mechatronics. 1996;**1**(1):1–4.

[2] Kyura N, Oho H. Mechatronics—an industrial perspective. IEEE/ASME Trans. Mechatronics. 1996;**1**(1):10–15.

[3] Bishop R H, editor. The Mechatronics Handbook, 2nd ed. CRC Press. New York. 2007.

[4] Ishihara H, Arai F, Fukuda T. Micro mechatronics and micro actuators. IEEE/ASME Trans. Mechatronics. 1996;**1**(1):68–79. DOI: 10.1109/3516.491411

[5] Kim C J, Pisano A P, Muller R S, Lim M G. Design, fabrication, and testing of a polysilicon microgripper. Microstruct. Sens. Actuators. 1990;**19**:99–109.

[6] Beyeler F, Neild A, Oberti S, Bell D J, Sun Y. Monolithically fabricated microgripper with integrated force sensor for manipulating microobjects and biological cells aligned in an ultrasonic field. J. Microelectromech. Sys. 2007;**16**(1):7–15. DOI: 10.1109/JMEMS.2006.885853

[7] Chang R J, Lin C Y, Lin P S. Visual-based automation of peg-in-hole microassembly process. Trans. ASME, J. Manu. Sci. Eng. 2011;**133**(041015):1–12. DOI: 10.1115/1.4004497

[8] Lu Z, Chen P C Y, Lin W. Force sensing and control in micromanipulation. Part C: applications and reviews. IEEE Trans. Sys., Man, Cyber. 2006;**36**(6):713–724. DOI: 10.1109/TSMCC.2006.879385

[9] Kim K, Liu X, Zhang Y, Sun Y. Nanonewton force-controlled manipulation of biological cells using a monolithic MEMS microgripper with two-axis force feedback. J. Micromech. Microeng. 2008;**18:**055013.

[10] Zhang Y, Chen B, Liu X, Sun Y. Autonomous robotic pick-and-place of microobjects. IEEE Trans. Robot. 2010;**26**:200–207. DOI: 10.1109/TRO.2009.2034831

[11] Chang R J, Shiu C C, Cheng C Y. Self-biased-SMA drive PU microgripper with force sensing in visual servo. Int. J. Adv. Rob. Sys. 2013;**10**(280):1–12. DOI: 10.5772/56643

[12] Chang R J, Lin Y C, Shiu C C, Hsieh Y T. Development of SMA-actuated microgripper in micro assembly applications. The 33rd Annual Conference of the IEEE Industrial Electronics Society (IECON). 2007. DOI: 10.1109/IECON.2007.4460001

[13] Clévy C, Hubert A, Chaillet N. Micromanipulation and Micro-Assembly Systems. IEEE/RAS Int. Adv. Robot. Program. (IARP'06). 2006.

[14] Sanchez-Salmeron A J, Lopez-Tarazon R, Guzman-Diana R, Ricolfe-Viala C. Recent development in micro-handling systems for micro-manufacturing. J. Mater. Proc. Tech. 2005;**167**:499–507.

[15] Fatikow S, editor. Automated Nanohandling by Microrobots. London: Springer. 2008.

[16] Judy J W. Microelectromechanical systems (MEMS): fabrication, design and applications. Smart Mater. Struct. 2001;**10**:1115–1134.

[17] Midha A, Norton T W, Howell L L. On the nomenclature, classification, and abstractions of compliant mechanisms. Trans. ASME J. Mech. Design. 1994;**116**:270–279. DOI: 10.1115/1.2919358

[18] Howell L L. Compliant Mechanisms. New York: Wiley. 2011.

[19] Cecil, J, Bharathi Raj Kumar M B, Lu Y, Basallali V. A review of micro-devices assembly techniques and technology. Int. J. Adv. Manuf. Technol. 2015;**83**(9):1569–1581. DOI: 10.1007/s00170-015-7698-6

[20] Suh N P. The Principles of Design. New York: Oxford University Press. 1990.

[21] Chang R J, Wang H S, Wang Y L. Development of mesoscopic polymer gripper system guided by precision design axioms. Precision Eng. 2003;**7**:362–369.

[22] Chang R J, Chen C C. Using microgripper in development of automatic adhesive glue transferring and binding microassembly system. Engineering. 2010;**1.2**(1):1–11. DOI: 10.4236/eng.2010.21001

[23] Brussel H V, Peirs J, Reynaerts D, Delchambre A, Reinhart G, Roth N, Weck M, Zussman E. Assembly of microsystems. CIRP Annals. 2000;**49**:451–472. DOI: 10.1016/S0007-8506 (07)63450-7

[24] Tichem M, Lang D, Karpuschewski B. A classification scheme for quantitative analysis of micro-grip principles. Assem. Autom. 2004;**24**(1):88–93.

[25] Kohl M. Shape Memory Microactuators. New York: Springer. 2004.

[26] Chang R J, Wang Y L. Integration method for input-output modeling and error analysis of four-bar polymer compliant micromachines. Trans. ASME J. Mech. Design. 1999;**121**:220–228. DOI: 10.1115/1.2829447

[27] Paros J M, Weisbord L. How to design flexure hinges. Mach. Des. 1965;**36**:151–156.

[28] Zhu P P, Cui Z W, Kesler M S, Newman J A, Manuel M V, Wright M C, Brinson L C. Characterization and modeling of three-dimensional self-healing shape memory alloy-reinforced metal-matrix composites. Mech. Mater. 2016;**103**:1–10.

[29] Gorbert R B. Control of hysteretic system with Preisach representation. Ph.D. Thesis. Canada: University of Waterloo. 1997.

[30] Mittal S, Menq C H. Hysteresis compensation in electromagnetic actuators through Preisach model inversion. IEEE/ASME Trans. Mechatronics. 2000;**5**(4):394–409. DOI: 10.1109/3516. 891051

[31] Bobál V, Böhm J, Fessl J, Macháček J. Digital Self-tuning Controllers. Berlin: Springer. 2005.

[32] Åström K J, Wittenmark B. Adaptive Control, 2nd ed. New York: Addision-Wesley. 1995.

IntechOpen